

# The quantum pulse gate – enabling high-dimensional time-frequency quantum information

Benjamin Brecht<sup>1\*</sup>, Andreas Eckstein<sup>1,2</sup>, Raimund Ricken<sup>1</sup>, Viktor Quiring<sup>1</sup>, Hubertus Suche<sup>1</sup>, Linda Sansoni<sup>1</sup>, and Christine Silberhorn<sup>1</sup>

*Integrated Quantum Optics, Applied Physics, University of Paderborn,  
Warburger Strasse 100 33098, Paderborn, Germany and*

*Laboratoire Matériaux et Phénomènes Quantiques, Université Paris Diderot - Paris 7,  
Bâtiment Condorcet, Case courrier 7021, 75205 Paris, France*

(Dated: March 19, 2014)

Time-frequency (TF) modes of ultrafast quantum states are naturally compatible with high bit-rate integrated quantum communication networks. Thus they offer an attractive alternative for the realization of high dimensional quantum optics. Here, we present a quantum pulse gate based on dispersion-engineered ultrafast frequency conversion in a nonlinear optical waveguide, which is a key element for harnessing the potential of TF modes. We experimentally retrieve the modal TF structure of our device and demonstrate a single-mode operation fidelity of 80%, which is limited by experimental shortcomings. In addition, we retrieve a conversion efficiency of 87.7% with a high signal-to-noise ratio of 8.8 when operating the quantum pulse gate at the single-photon level.

The advent of the field of quantum information and computation has changed our way of thinking about information. The concept of mutually unbiased bases (MUBs) [1] lies at the heart of quantum information science applications like quantum key distribution [2], quantum state tomography [3] or entanglement detection [4]. Most of these applications concentrate on two-dimensional systems, without exploiting the full potential of quantum mechanics. Only recently, people have suggested utilizing higher-dimensional bases, which are of fundamental interest for questions addressing nonlocality [5, 6]. In addition, they facilitate larger alphabets, which promise increased security for quantum cryptography [7, 8]. A major requirement for any implementation of high-dimensional coding is a device which grants access to different basis states, in order to perform measurements in different MUBs.

To date, the most widely used approach to exploit high-dimensionality is to deploy the orbital angular momentum (OAM) of photon pairs generated in parametric down-conversion (PDC) [9–11]. Recent results demonstrated an increased information capacity [12] and increased security for quantum cryptography [13, 14], as was predicted for high-dimensional coding.

OAM states are appealing basis states, because they form a *natural* basis for describing spatial entanglement in PDC [15, 16]. In addition, there exists an efficient mode sorter, which facilitates the deterministic separation of many OAM states using only linear optical elements [17]. On the downside, OAM states are incompatible with integrated single-mode network architectures, because they encode information in different spatial field modes. This directly implies, that OAM states cannot be generated with waveguided PDC sources, which feature high brightness and excellent compatibility with fiber networks [18].

However, PDC provides an alternative resource for

high-dimensional information coding, namely energy-time entanglement [19, 20]. Here, the *natural* basis functions are the so-called Schmidt modes or time-frequency (TF) modes [21]. Compared to OAM states, TF modes offer three advantages for high-dimensional information coding: first, they are well-suited to integration, because they all live within the same spatial field distribution; second, a sophisticated toolbox for controlling the TF structure of PDC exists [22], and results on waveguided PDC have already demonstrated the energy-efficient generation of single- and few-mode states with tunable TF correlations [18, 23]; third, waveguided PDC guarantees and intrinsic control over the spatial degree of freedom, which is largely decoupled from the spectrum [24].

The drawback of TF modes is, that their manipulation cannot be accomplished with linear optical elements, and a mode sorter has not been available. As an answer to this, we have recently proposed a so-called quantum pulse gate (QPG) that is capable of selecting a single TF mode from a high-dimensional input and convert it to a different frequency [25, 26].

In this paper, we present the experimental implementation of a QPG: we demonstrate TF single-mode operation with a fidelity of up to 80%, and present a way of retrieving the QPG TF mode structure in the experiment. Moreover, we measure a conversion efficiency of close to 90% when operating the device at the quantum level. Similar to the mode sorter for OAM states, we expect our device to become an enabling technology for high-dimensional quantum information applications based on TF modes.

The QPG is based on dispersion-engineered, ultrafast sum-frequency generation in a periodically poled lithium niobate waveguide. Due to the careful tailoring of the device, the input signal propagates through the waveguide at the same velocity as the pump pulses. In this case,

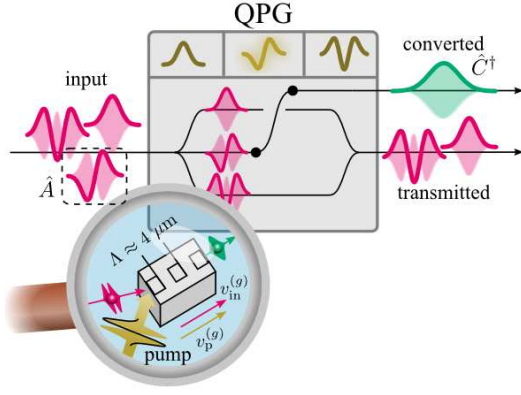


FIG. 1. Illustration of a QPG. A single TF  $\mathcal{A}(\omega)$  mode from a multimode input state is selected and converted to an output mode  $\mathcal{C}(\omega)$  at a different frequency. The remaining modes are simply transmitted. For more information see the text.

the QPG operation on an input state  $|\psi\rangle_{\text{in}}$  is given by

$$|\psi\rangle_{\text{out}} = \exp \left[ \theta \hat{A} \hat{C}^\dagger + \text{h.c.} \right] |\psi\rangle_{\text{in}}, \quad (1)$$

where the operators  $\hat{A}$  and  $\hat{C}^\dagger$  are TF mode operators [21]. They describe the annihilation of a photon in an ultrafast pulse with spectrum  $\mathcal{A}(\omega)$  and the simultaneous generation of a photon in a pulse with spectrum  $\mathcal{C}(\omega)$ , which is centred at a different frequency.

The working principle of a QPG is illustrated in Fig. 1. A TF multimode input state (left) is sent into a QPG, which is adapted such that the highlighted TF mode  $\hat{A}$  is selected and converted into  $\hat{C}^\dagger$ . The remaining TF modes of the input are transmitted. The magnified view shows the underlying device. Ultrafast, shaped pump pulses (yellow), which serve as a dial choosing the selected mode, are coupled to a periodically poled nonlinear waveguide, together with the input (red). Inside the waveguide, pump and input propagate at the same group velocity and a converted output is generated at the sum-frequency of input and pump. At the output of the QPG, converted and transmitted TF modes can be separated using a dichroic mirror. Note that the shape of the selected TF mode  $\hat{A}$  is defined by the shape of the ultrafast pump pulses of the QPG, whereas the converted mode  $\hat{C}^\dagger$  is given by the waveguide dispersion.

The QPG can be interpreted as a special quantum mechanical beamsplitter, which operates on a single TF mode of an ultrafast quantum state. The reflectivity or conversion efficiency of the QPG is given by  $\sin^2(\theta)$  (compare Eq. (1)), where the coupling constant  $\theta$  is a function of the pump power and complete conversion is, in principle, possible.

The general idea to verify the QPG operation in the experiment, is to perform a tomographic reconstruction of the modal TF characteristics of the QPG. In contrast to quantum process tomography, where photon-number

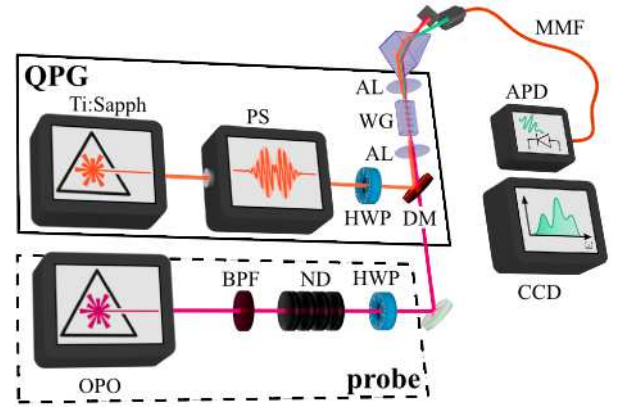


FIG. 2. Experimental setup. PS, pulse shaper; OPO, optical parametric oscillator; BPF, bandpass filter; ND, neutral density filter; HWP, half-wave plate; DM, dichroic mirror; AL, aspheric lens; WG, waveguide sample; MMF, multimode fiber; APD, avalanche photo diode; CCD, single-photon sensitive CCD spectrometer. For more information see the text.

properties of the process are evaluated [27], modal characteristics have the advantage that they are a mutual concept of classical and quantum light. Consequently they are accessible with *classical* measurements only. This can also be seen from Eq. (1), where the QPG operation is independent of the actual choice of input states. In particular, the operation is valid for single-photon input as well as for continuous-variable states exhibiting higher photon numbers and even coherent states. This facilitates the complete characterization of the TF mode structure by evaluating the impact of the QPG on a set of coherent probe states, which significantly simplifies the experimental effort. As a side-remark we point out that, for this work, probing one QPG with a set of probe states is tantamount to probing many different QPGs with one single probe state. In our measurements, we chose the latter option due to experimental simplicity.

Our coherent probe state exhibited a Gaussian TF mode  $\hat{G}^\dagger$ , with an associated spectral distribution  $\mathcal{G}(\omega)$ . In addition, we implemented different QPGs by shaping of the classical pump pulses, thus changing the selected mode  $\hat{A}$ . Then, the QPG only selects the fraction of the probe that overlaps with  $\hat{A}$ . Consequently, the converted output intensity is proportional to  $I_{\text{out}} \propto |\int d\omega \mathcal{G}(\omega) \mathcal{A}^*(\omega)|$ . Note that, although the measured quantity is an intensity, our approach is inherently phase-sensitive, since the overlap integral contains the complex-valued TF mode spectra. In this way, it is possible to map the selected mode  $\hat{A}$  by monitoring  $I_{\text{out}}$  for different realizations of the QPG. In contrast, the spectrum of the converted output is given by  $\mathcal{C}(\omega)$  and thus grants direct access to the output mode  $\hat{C}^\dagger$ .

Our experimental setup is shown in Fig. 2. We labeled the different sections of the setup corresponding to the elements in Fig. 1. An optical parametric oscillator

(APE Compact OPO) generated ultrafast pulses with a central wavelength of 1535 nm, which were subsequently filtered to a spectral bandwidth of 12 nm, corresponding to a pulse duration of 287 fs. Several neutral density filters attenuated the pulses to the single-photon level. After adjusting their polarization, the pulses were deployed as probe states for the QPG. The second part of the setup, the actual QPG, consists of a titanium sapphire oscillator (Coherent Chameleon Ultra II) generating 865 nm pulses with a maximum bandwidth of 7.9 nm, corresponding to a duration of 140 fs, which served as bright pump for the QPG. The pulses were sent through an acousto-optic pulse shaper (Fastlite Dazzler) to realize different pulse shapes and subsequently coupled to the waveguide sample. We deployed a homemade periodically poled waveguide with a remarkably low poling period of only 4.4  $\mu\text{m}$ , which was temperature stabilised at  $T = 190^\circ\text{C}$  to provide quasi-phases-matching between the involved fields and at the same time minimize detrimental photorefractive effects. Behind the waveguide, a prism setup implemented spectral filtering of the generated output light at  $\lambda_{\text{out}} = 553 \text{ nm}$ . Then, the light was coupled into a multimode fiber, which was fed into either a single-photon sensitive CCD spectrometer (Andor iKon-M 934P-DD / Shamrock SR-303iA), or a silicon avalanche photo diode (Perkin Elmer SPCM-AQRH-13) for photon counting.

In the following, we present our measurement results. First, we concentrated on the experimental characterisation of the QPG TF mode structure, which at the same time facilitates the identification of the ideal QPG operation wavelength. Thereafter, we adapt the QPG bandwidth to our unknown probe state. Having found the ideal operation point, we perform a benchmarking of the QPG performance both in terms of mode selection and conversion efficiency at the single-photon level.

Our first measurements disclose the QPG TF mode structure. In addition, they are the first step towards adapting the QPG to an unknown input state. We utilized bright probe pulses with around 100 photons per pulse and realized different QPGs by shaping the pump pulses into four different Hermite-Gaussian modes with durations of 150 fs, which intentionally do not fit to the probe state. The Hermite-Gaussian functions form a complete basis, which fits to the Gaussian TF mode  $\mathcal{G}(\omega)$  of our probe state. For each QPG implementation, we scanned the central pump wavelength between 855 nm and 872 nm and recorded the converted output spectra with the CCD spectrometer.

The resulting spectra are shown in Fig. 3(a), where we restrict ourselves to spectra for chosen pump wavelengths for better readability. From top left to bottom right, the basic TF shape of the pump changes from a fundamental Gaussian to a third-order Hermite-Gaussian. From our theory we expect that the output TF mode  $\hat{C}^\dagger$  of the QPG is only defined by the phasematching of the wave-

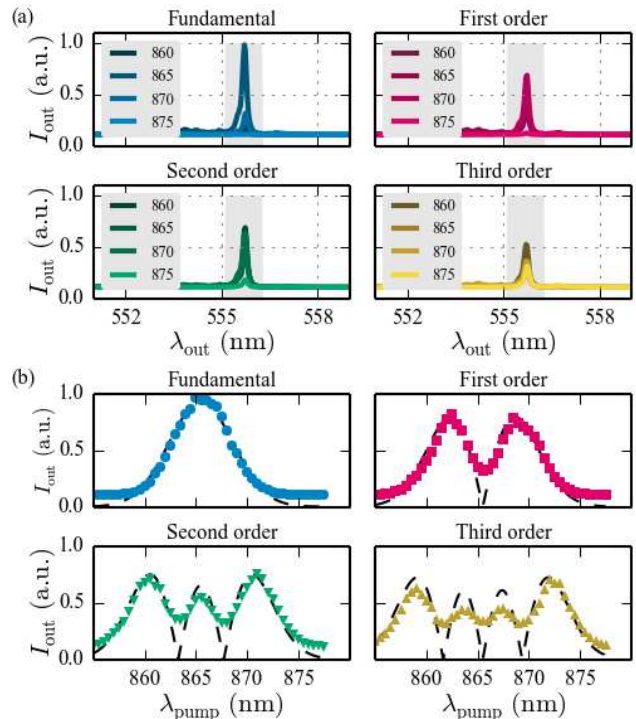


FIG. 3. Measurement results for the reconstruction of the QPG TF modes. In (a), we plot chosen recorded output spectra for the indicated pump wavelengths, whereas in (b) we show the converted output intensity  $I_{\text{out}}$  as a function of the pump wavelength  $\lambda_{\text{p}}$ . Note that error bars in (b) are smaller than the symbols. For more information see the text.

uide. This is verified by the measured spectra, which are similar regardless of the pump TF shape. For applications this means, that formerly orthogonal TF modes can be interfered after the QPG operation.

From the measured spectra we retrieve a spectral bandwidth of  $\Delta\lambda_{\text{out}} \approx 0.14 \text{ nm}$ , corresponding to a pulse duration of 3.2 ps, which demonstrates a bandwidth compression during the conversion about a factor of eleven. This intrinsic feature of our device is of interest for applications aiming for interfacing photons and quantum memories, which typically feature narrow acceptance bandwidths. Note that, although higher values of compression have been reported in the literature [28], the QPG provides this number without additional experimental effort, and an even larger compression can be realized by deploying longer waveguides.

In Fig. 3(b), we plot the output intensities  $I_{\text{out}}$  as a function of the pump wavelength  $\lambda_{\text{p}}$ . The intensities were calculated from the spectra by integrating over the grey-shaded area in Fig. 3(a). From top left to bottom right, the pump TF shape again changes from a fundamental Gaussian to a third-order Hermite-Gaussian. We recall that  $I_{\text{out}} \propto |\int d\omega \mathcal{G}(\omega) \mathcal{A}^*(\omega)|$ , and find that the measured curves nicely reproduce the pump TF shape, indicated by the dashed black lines in the respective di-



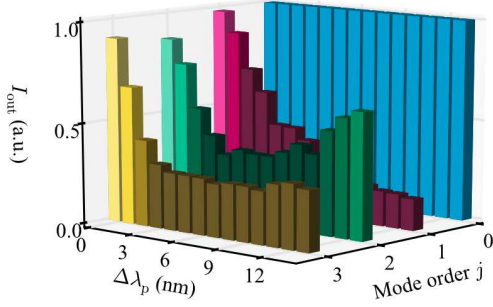


FIG. 4. Measurement results for the adaption of the QPG TF modes to an unknown input. For more details see the text.

agrams. Deviations occur only in the regions of sharp features, which we can attribute to the limited resolution of the pulse shaper of  $\Delta\lambda_{\text{PS}} = 0.7$  nm. Hence, this measurement demonstrates that the input mode  $\hat{A}$  is really defined by the shape of the ultrafast pump pulses, as was expected from theory (for more details, see the supplementary material).

We also identify an ideal central pump wavelength at  $\lambda_p = 865.6$  nm, where the conversion for the Gaussian is highest, and similarly the conversion for the first-order mode exhibits a minimum. Thus, by probing the QPG with a coherent state, we succeeded in retrieving the QPG TF mode structure as well as in adapting the central QPG wavelength to our input state.

In the next measurement, we demonstrate the second step towards optimization of  $\hat{A}$  with respect to the probe state. We fixed the central pump wavelength at the optimal value of  $\lambda_p = 865.6$  nm and changed the spectral pump bandwidth  $\Delta\lambda_p$ . Again, we recorded the output intensity for the different pump TF shapes from Fig. 3.

Note that we do not expect to measure any conversion for odd-order pump modes, because they do not have an overlap with the even TF mode  $\hat{G}^\dagger$  of the probe state, regardless of their spectral bandwidths. In contrast, the overlap between a second-order Hermite-Gaussian pump and the probe only vanishes for an ideally adapted pump bandwidth.

Our measurement results are shown in Fig. 4, where we plot the output intensity  $I_{\text{out}}$ , normalized to the efficiency achieved with the fundamental TF pump mode, against the pump bandwidth. The normalization was unavoidable, because the pulse shaper did not guarantee similar pump pulse energies when switching between different spectral widths. As expected, the conversion efficiency for the odd order pump modes drops to a minimum after the resolution limit of the pulse shaper is overcome, and does not increase again. In contrast, the conversion efficiency for the second-order pump mode decreases to a minimum and then starts to increase again, when further increasing  $\Delta\lambda_p$ . From the measurements, we deduce an *ideal* pump bandwidth of  $\Delta\lambda_p \approx 4.0$  nm,

corresponding to a pump duration of around 275 fs. This is in excellent agreement with the duration of the probe pulses of 287 fs, as we would have expected.

Our final measurements aim for the performance benchmarks of the QPG. To this end, we fixed the pump parameters at the optimized values of  $\lambda_p = 865.6$  nm and  $\Delta\lambda_p = 4.0$  nm, which we obtained from our two-step method describe before. Then, we again switched the pump mode from Gaussian to first-order Hermite-Gaussian and recorded the converted output spectrum. This measurement is shown in Fig. 5 (a). The blue spectrum corresponds to a Gaussian pump (top inset), whereas the red spectrum was taken with a Hermite-Gaussian pump (bottom inset), respectively. When subtracting the flat spectral background, marked as grey area, we obtain a suppression or *mode-selectivity* of 80%, which is limited by the finite resolution of the pulse shaper.

Finally, we investigated the noise performance and conversion efficiency of the QPG when operated at the single photon level. Therefore, we attenuated the probe states to a mean photon number of  $\langle n \rangle \approx 0.15$  photons/pulse and recorded the converted output counts with the APD. The results are shown in Fig. 5 (b), where we plot the recorded counts versus the pump pulse energy. We retrieved the background counts by blocking the probe state and recording the remaining counts for each pump energy, and find that the background corrected counts (green squares) are in excellent agreement with the theoretical  $\sin^2$ -fit. In addition, the signal-to-noise ratio for maximum conversion is 8.8, which demonstrates a low-noise operation of the QPG. We deduce an internal conversion efficiency, defined as the number of converted photons at the end of the waveguide versus number of probe photons at the input, of 87.7%, where we did not correct for waveguide propagation losses. This maximum is reached at a pump pulse energy of only  $E_p \approx 16$  pJ in front of the waveguide incoupling, corresponding to a cw-equivalent power as low as 1.3 mW for 80 MHz repetition rate. This remarkable efficiency is possible only due to the careful tailoring of our device. Since pump and probe pulses propagate through the waveguide at the same velocity, the probe always experiences the high peak power of the pump pulses. In addition, the TF single-mode behavior facilitates an extra-ordinary energy efficiency, which becomes a key feature when considering large-scale quantum networks.

In conclusion, we implemented a QPG and retrieved its modal TF characteristics by probing it with coherent probe states. Our device facilitates a single-mode operation on the TF modes of ultrafast quantum states, with a mode-selectivity of at least 80%, limited mainly by the finite resolution of our pulse shaper. This operation facilitates measurements of the TF degree of freedom in different, high-dimensional mutually unbiased bases, which is a prerequisite for many quantum information applica-

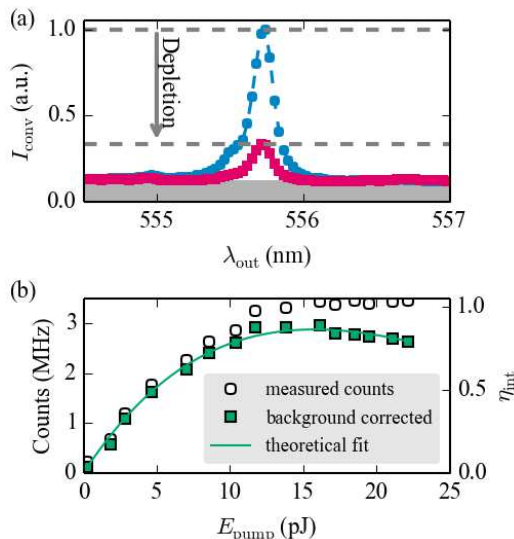


FIG. 5. Performance benchmarks of our QPG. From the spectral suppression in (a), we obtain a mode-selectivity of 80%, whereas the efficiency measurement in (b) reveals an internal conversion efficiency of 87.7%. In both plots, error bars are smaller than the symbols. For more information see the text.

tions, for instance quantum cryptography with increased security [13, 14]. In addition, our device provides a high internal conversion efficiency of 87.7% and a good signal-to-noise ratio of 8.8 when operated at the single photon level. Since the output mode of the QPG is independent of the selected mode, the QPG facilitates interfacing between orthogonal TF modes. Moreover, when operated at low conversion efficiencies, the QPG can be exploited for the implementation of TF mode-selective non-Gaussian operations in multimode continuous-variable quantum information schemes. Hence, we expect our work to have a considerable impact on a wide range of applications in discrete and continuous variable quantum information.

The authors acknowledge helpful discussion with Andreas Christ, Fabian Katzschmann and Michael Stefszky. The authors acknowledge funding from the European Community's Seventh Framework Programme FP7/2001-2013 under grant agreement no. 248095 through the Integrated Project Q-ESSENCE.

[1] J. Schwinger, Proceedings of the National Academy of Sciences of the United States of America **46**, 570 (1960).

[2] C. H. Bennett and G. Brassard, in *Proceedings of IEEE International ...* (1984).  
 [3] D. Smithey, M. Beck, M. Raymer, and A. Faridani, Physical Review Letters **70**, 1244 (1993).  
 [4] C. Spengler, M. Huber, S. Brierley, T. Adaktylos, and B. C. Hiesmayr, Physical Review A **86**, 022311 (2012).  
 [5] D. Collins, N. Gisin, N. Linden, S. Massar, and S. Popescu, Physical Review Letters **88** (2002).  
 [6] T. Vértesi, S. Pironio, and N. Brunner, Physical Review Letters **104**, 060401 (2010).  
 [7] H. Bechmann-Pasquinucci and W. Tittel, Physical Review A **61** (2000).  
 [8] N. J. Cerf, M. Bourennane, A. Karlsson, and N. Gisin, Physical Review Letters **88**, 127902 (2002).  
 [9] A. Mair, A. Vaziri, G. Weihs, and A. Zeilinger, Nature **412**, 313 (2001).  
 [10] J. Leach, B. Jack, J. Romero, A. K. Jha, and A. M. Yao, Science **329**, 662 (2010).  
 [11] A. C. Dada, J. Leach, G. S. Buller, M. J. Padgett, and E. Andersson, Nature Physics **7**, 677 (2011).  
 [12] J. T. Barreiro, T.-C. Wei, and P. G. Kwiat, Nature Physics **4**, 282 (2008).  
 [13] S. Gröblacher, T. Jennewein, A. Vaziri, G. Weihs, and A. Zeilinger, New Journal of Physics **8**, 75 (2006).  
 [14] J. Leach, E. Bolduc, D. J. Gauthier, and R. Boyd, Physical Review A **85**, 060304 (2012).  
 [15] H. Arnaut and G. Barbosa, Physical Review Letters **85**, 286 (2000).  
 [16] S. Franke-Arnold, S. Barnett, M. Padgett, and L. Allen, Physical Review A **65**, 033823 (2002).  
 [17] G. C. G. Berkhout, M. P. J. Lavery, J. Courtial, M. W. Beijersbergen, and M. J. Padgett, Physical Review Letters **105**, 153601 (2010).  
 [18] G. Harder, V. Ansari, B. Brecht, T. Dirmeier, C. Marquardt, and C. Silberhorn, Optics Express **21**, 13975 (2013).  
 [19] J. D. Franson, Physical Review Letters (1989).  
 [20] P. G. Kwiat, A. M. Steinberg, and R. Y. Chiao, Physical Review A **47**, R2472 (1993).  
 [21] C. K. Law, I. A. Walmsley, and J. H. Eberly, Physical Review Letters **84**, 5304 (2000).  
 [22] A. B. U'Ren, C. Silberhorn, K. Banaszek, I. A. Walmsley, R. Erdmann, W. P. Grice, and M. G. Raymer, Laser Phys. **15**, 146 (2005).  
 [23] A. Eckstein, A. Christ, P. J. Mosley, and C. Silberhorn, Physical Review Letters **106**, 13603 (2011).  
 [24] P. Mosley, A. Christ, A. Eckstein, and C. Silberhorn, Physical Review Letters **103** (2009).  
 [25] A. Eckstein, B. Brecht, and C. Silberhorn, Optics Express **19**, 13370 (2011).  
 [26] B. Brecht, A. Eckstein, A. Christ, H. Suche, and C. Silberhorn, New Journal of Physics **13**, 065029 (2011).  
 [27] M. Lobino, D. Korystov, C. Kupchak, E. Figueroa, B. C. Sanders, and A. I. Lvovsky, Science **322**, 563 (2008).  
 [28] J. Lavoie, J. M. Donohue, L. G. Wright, A. Fedrizzi, and K. J. Resch, Nature Photonics **7**, 363 (2013).